JOURNAL OF MATERIALS SCIENCE **38** (2003) 3037–3050

# Detection of martensite transformation in high temperature compressively deformed austenitic stainless steel by magnetic NDE technique

K. MUMTAZ, S. TAKAHASHI, J. ECHIGOYA, LF. ZHANG, Y. KAMADA, M. SATO
*Non-Destructive Evaluation and Science Research Center, Faculty of Engineering, Iwate University, Morioka-020-8551, Japan*
*E-mail: fahadkm@iwate-u.ac.jp*

The present work demonstrates that a magnetic non-destructive evaluation technique can be useful for detecting the presence and extent of ferromagnetic $\alpha'$ martensitic phase in high temperature deformed 304 austenitic stainless steel.

A good correlation between the martensitic transformation and magnetic parameters; saturation magnetization, coercive force and magnetic susceptibility have been obtained. Saturation magnetization was increased depending on the volume percentage of $\alpha'$ martensite transformation. The volume percentage of $\alpha'$ martensite was found to be dependent on the temperature and level of plastic strain. At temperatures below 623 K, martensitic transformation was detected after deformation of 10 to 40% plastic strain. A massive increase in $\alpha'$ martensite phase was observed in the specimen deformed at RT to 40% plastic strain.

Compressive deformation at RT formed thermodynamically more stable long and broad shape of martensite. But as the temperature of deformation increases lath shape gradually converted into needle shape.

Coercive force was exclusively connected with size, shape and spatial distribution of martensite. For specimens deformed at 523 K coercive force were much higher than those of the specimens deformed at RT. Coercive force decreased remarkably at temperatures above 623 K. Formation of ferromagnetic $\alpha'$ martensite in a paramagnetic matrix was also accompanied by an increase in magnetic susceptibility. Low magnetic susceptibility at temperatures above 623 K was due to disappearance of martensitic phase. 

## 1. Introduction

Austenitic stainless steels are widely used in nuclear power plants to construct pipelines and vessels operated at high temperature and pressure [1–5]. It has been observed that after long-term of service, the austenitic stainless steel is likely to crack and cause a series of disasters in some boiling water reactor and pressurized water reactor nuclear power generating systems. Irradiation and fatigue damage are two major phenomena present in nuclear power plant. Stresses that develop during irradiation cannot be prevented. The combination of mechanically and/or thermally induced stresses and poor ductility are responsible for several form of cracks. The cracks are produced from a pile of dislocations, where the dislocation density becomes maximum locally [6–9]. In the current practice, we have many methods to detect presence of crack, such as X-ray diffraction, eddy current detection, magnetic particle testing and acoustic emission [5, 6, 10–13], but there are no non-destructive means to determine the degradation of material before crack initiation. Therefore, in order to meet the industry increasing demands for safe operation of nuclear power plant, researchers are trying their best to find a practical method to evaluate the degradation of stainless steel structures during operation.

The degradation of materials relate to the changes in microstructure and chemical composition within materials. Temperature, stress, strain etc. influenced the value of some chemical or physical properties of materials [14]. And on the other side, variation of chemical or physical properties can reflect the change in materials. Magnetic property is one of the most sensitive to the change in physical properties of materials.

In stainless steel and ferromagnetic materials changes in physical properties reflect degradation of structural integrity before crack initiation, a technique that could correlate magnetic behavior with physical properties would be a valuable non-destructive evaluation (NDE) tool. Therefore, there is current interest in the use of measurements of magnetic properties as a NDE tool for monitoring and determining deformation

and damage prior to crack initiation, in austenitic stainless steel [15, 16]. By monitoring the amount and nature of phase changes occurring in stainless steel structures, one can determine when to take preventive measures and, perhaps, in what ways to intervene at early stages of the process. Thus the risk of cracking can be minimized while at the same time increasing reliability of nuclear power plants.

In nuclear power plants, stainless steel pipes usually operate in the environment of pressurized hot water at temperatures between 473 K and 623 K. Fatigue and nuclear radiation are also affect reactor components made of stainless steel. After the materials have given a long-term of service, there may be composition segregation, metallic compound precipitation, grain boundary oxidization, interior defects like dislocation and stacking fault and martensitic transformation. These effects may cause the materials to degrade, and cracks can be produced at the weakest site. As has been mentioned before, magnetic properties are very sensitive to microstructural and compositional changes in materials, hence, by detecting the magnetic properties, such as saturation magnetization, coercive force, magnetic susceptibility, etc., we can probably get the evidence of degradation in materials [15–17].

It has been reported that the degradation of austenitic steel is always accompanied by martensitic transformation. Previous studies concerning martensitic transformation in austenitic stainless steels were mostly accomplished utilizing TEM and XRD techniques at low or cryogenic temperature [17–25]. However, TEM and XRD have certain limitations in cases when the amount of martensite phase is low. In this work, SUS 304 austenitic stainless steel were studied by using super conducting quantum interference device (SQUID) magnetometer and vibrating sample magnetometer (VSM) which are the latest high precision instruments for magnetic testing. We want to establish a quantitative correlation between the martensitic transformation and magnetic parameters after compressive deformation to 10% to 40% plastic strain at temperatures between room temperature (RT) and 723 K.

## 2. Experimental procedure

The material used for this investigation was SUS 304 austenitic stainless steel supplied by Nilaco Corporation Japan. The chemical composition of austenitic stainless steel used for the investigation is shown in Table I.

The as-received state of the material is cold-rolled plate stock, 100 mm length, 50 mm width and 2 mm in thickness. Compressive test specimens were prepared from plate parallel to the rolling direction by spark wire cutting machine (Fine Sodick Wire Cut EDM).

For compressive deformation test, specimens of size $3 \times 3 \times 2$ mm$^3$ were used. The average grain size of as-received specimens was about 30 $\mu$m (Fig. 1a). The specimens were first solution annealed in a vacuum furnace at temperature of 1323 K for 1 h and then water quenched. After the homogenization treatment, specimens were polished to 6000 grit emery paper. In order to remove the effect of polishing on the martensitic transformation, the specimens were electro-polished using a 170 ml : 30 ml solution of ethanol and perchloric acid at 30 V for 45 sec prior to compressive deformation. After solution annealing, the average grain size became about 115 $\mu$m as shown in Fig. 1b.

TABLE I Chemical composition of SUS 304 austenitic stainless steel

| Element | C | Cr | Ni | Mn | Si | P | S | Fe |
|---|---|---|---|---|---|---|---|---|
| Content wt% | 0.06 | 18.44 | 8.33 | 1.16 | 0.43 | 0.033 | 0.009 | Bal. |

Compressive deformation tests were performed on a Shimadzu Autograph Type SFL-250kN AG testing machine. Before each test, the specimen was heated to test temperature at a rate of 300 K/min and then held for 5 min. At the increment of 50 K, 10 levels of testing temperature from RT to 723 K were chosen. During the compression test, a strain rate of 0.5 mm/min was used to compress the specimens to get 10%, 20%, 30% and 40% plastic strain. After the compression test, the specimens were cooled in air. Before magnetic measurements specimens were once again hand and electro polished.

The saturation magnetization values were obtained from magnetization curves using a Design MPMS XL SQUID magnetometer at RT in applied field of 0 to 30 kOe. The coercive force was obtained from magnetic hysteresis loops with a VSM at RT in the applied magnetic field of $-20$ to $+20$ kOe.

X-ray diffraction (XRD) was carried out on the specimens to determine the crystallographic features and volume percentage of $\alpha'$ martensite phase using a Material Analysis and Characterization M 21X diffractometer with Cu K$\alpha$ radiation. The degree of martensitic transformation was quantified by comparison of the integrated intensity ratios of the ($\gamma$) austenite and ($\alpha'$) martensite reflections.

The microstructures were characterized using JEOL scanning electron microscope (SEM). For SEM examination a mixture of nitric acid and hydrochloric acid (1:3) solution was used to etch the specimens.

Following the magnetic measurements and X-ray diffraction tests, the microstructures were also characterized using transmission electron microscope (TEM). TEM bright field (BF) and dark field (DF) imaging were carried out using a Philips Technai-30 instrument with a double tilt holder operated at 200 kV. The TEM specimens were prepared parallel to the surface (planar section) of specimens. Thin foils were prepared by cutting thin slices. These slices were then ground to roughly 100 $\mu$m. Subsequent thinning was carried out by twin jet electro-polishing in a solution of perchloric acid and acetic acid (volume ratio was 1:9) at the voltage of 40 to 45 V.

## 3. Results and discussion

### 3.1. Stress-strain curve

The stress-strain curves at RT are shown in Fig. 2. As shown in the figure, the curves for specimens compressed at RT to 10% to 40% plastic strain are superimpose and show the same deformation behavior at different levels of strain. A similar trend was also

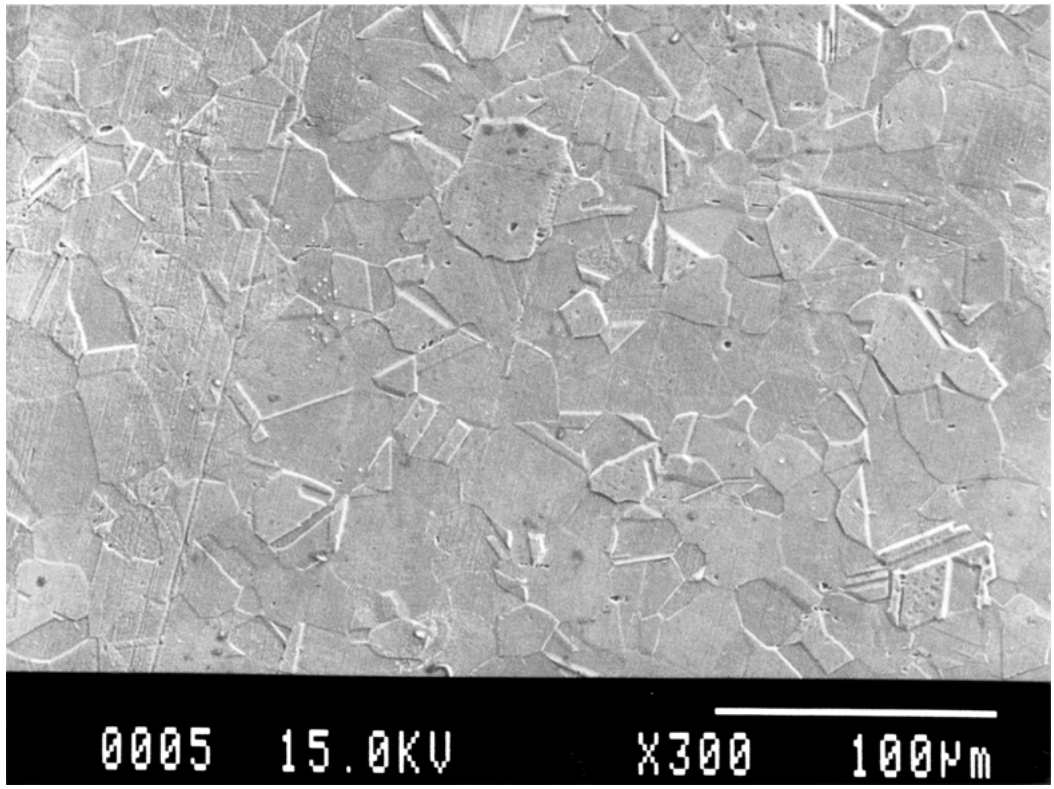


(a)

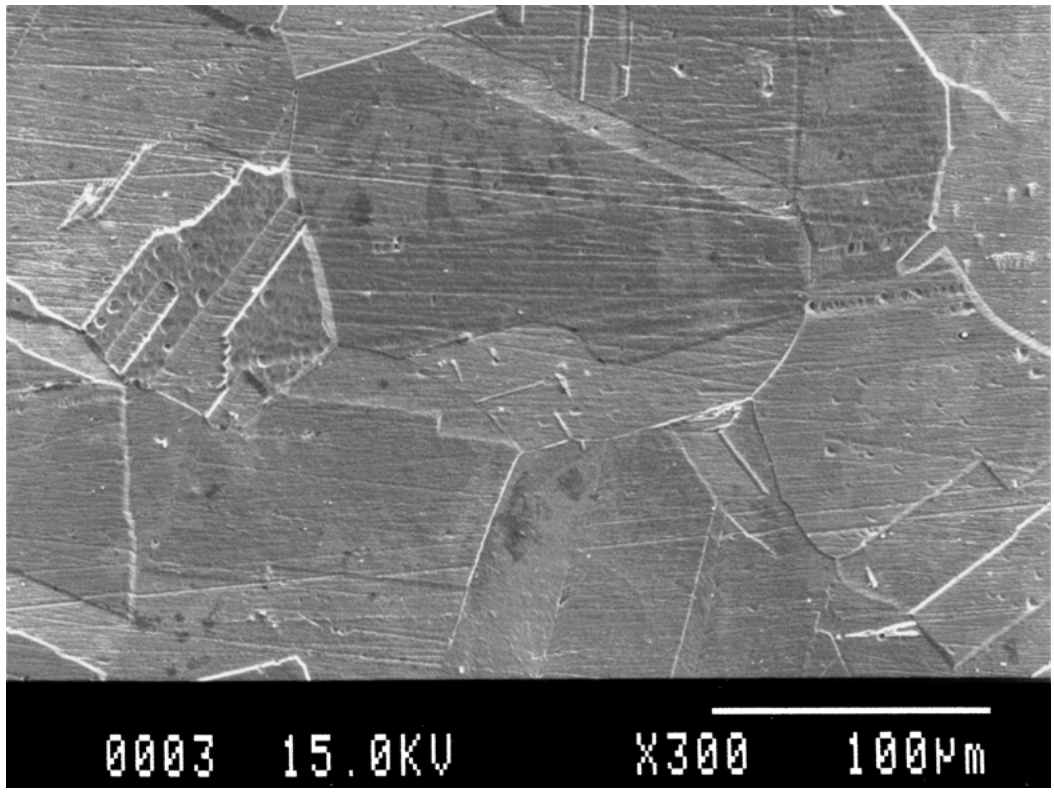


(b)

*Figure 1* SEM micrographs of SUS 304 stainless steel showing the equiaxed grain structure (a) as-received and (b) solution annealed (1323 K, 1 h).

observed in the specimens compressed at various temperatures to 10% to 40% plastic strain.

The stress-strain curves for compression tests performed at RT to 723 K to 40% plastic strain are shown in Fig. 3, relevant data is given in Table II. In the figure, three different stages of deformation in austenitic stainless steel can be seen. Stage A represents elastic deformation of the austenitic phase. In Stage I, the austenite to martensite transformation occurs at a slow rate. Stage II corresponds to martensitic transformation due to build-up of dislocation structure produces an increase in stress-strain slopes [26].

The influence of temperature on the yield stress of austenitic stainless steel to 40% plastic strain is shown

TABLE II Mechanical properties of austenitic stainless steel after compressive deformation at various temperatures to 40% plastic strain

| Specimen no. | Deformation temp. (K) | Max. stress (MPa) | Yield stress (MPa) | Hardening rate |
|---|---|---|---|---|
| SS-56 | RT | 2023 | 280 | 0.76805 |
| SS-60 | 323 | 1682 | 250 | 0.7628 |
| SS-64 | 373 | 1523 | 245 | 0.65617 |
| SS-68 | 423 | 1355 | 235 | 0.60381 |
| SS-72 | 473 | 1233 | 210 | 0.56458 |
| SS-76 | 523 | 1167 | 190 | 0.49119 |
| SS-80 | 573 | 1082 | 180 | 0.4623 |
| SS-84 | 623 | 1046 | 140 | 0.44745 |
| SS-88 | 673 | 953 | 105 | 0.43288 |
| SS-92 | 723 | 954 | 95 | 0.42424 |

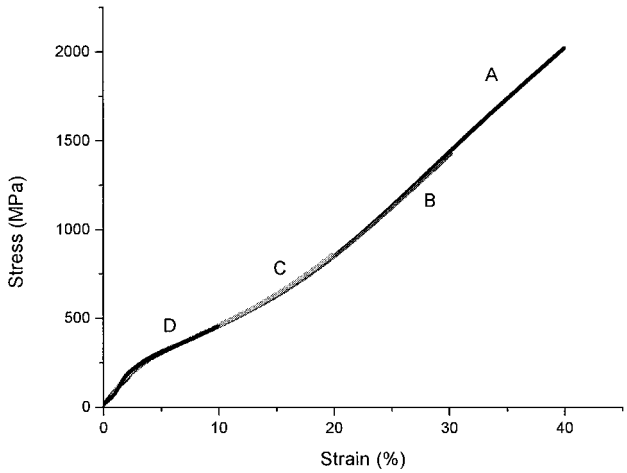


*Figure 2* Stress-strain curves of austenitic stainless steel compressed at RT with A = 10%, B = 20%, C = 30% and D = 40% plastic strain.

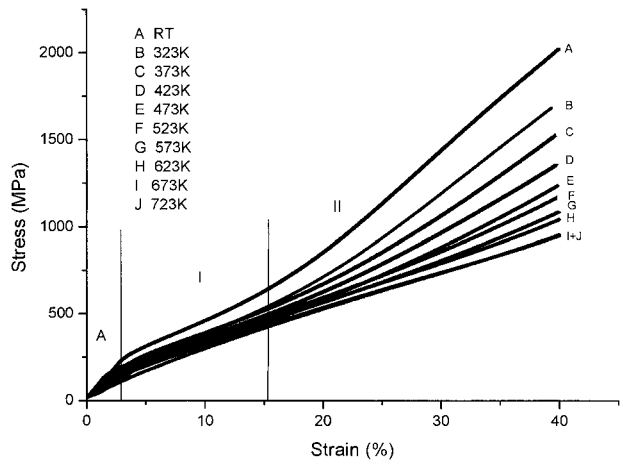


*Figure 3* Stress-strain curves of austenitic stainless steel compressively deformed at various temperatures to 40% plastic strain.

in Fig. 4. The yield stress decreased with the increase of temperature. At temperatures higher than 623 K, yield stress decreased drastically. Yield stress of 280 MPa and 95 MPa are obtained at RT and 723 K, respectively i.e., yield stress at RT is about three times higher than at 723 K.

Hardening rate of the austenitic stainless steel at different temperatures to 40% plastic strain is shown in Fig. 5. Hardening rate $n$ is calculated from the true stress $\sigma$, and true strain $\varepsilon_t$ values according to the fol-

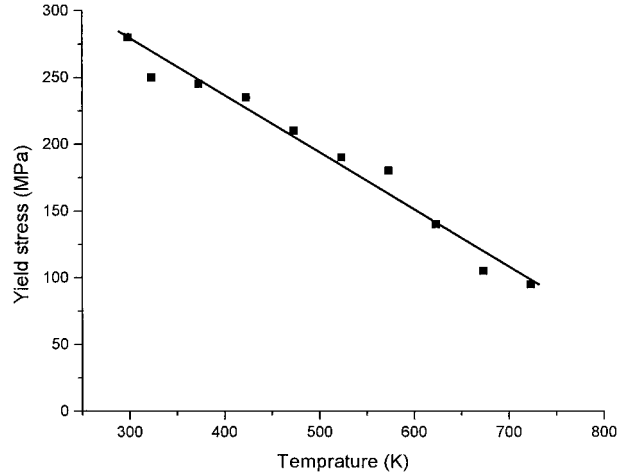


*Figure 4* Variation of yield stress with temperature for specimens compressively deformed to 40% plastic strain.

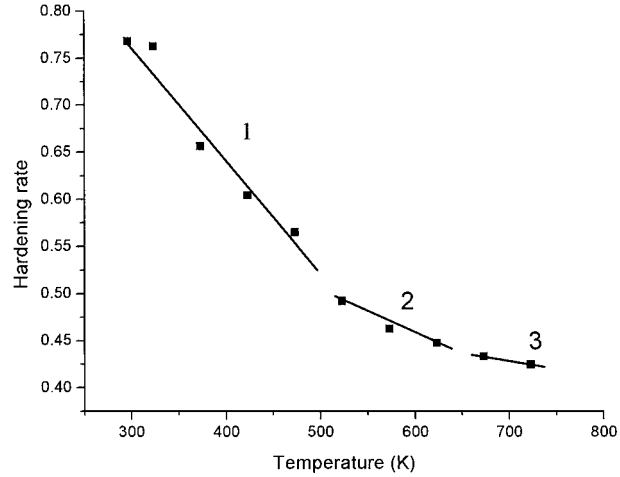


*Figure 5* Changes in hardening rate with temperature for specimens compressively deformed to 40% plastic strain.

lowing equation [27]:

$$\sigma_t = A\varepsilon_t^n \tag{1}$$

where $A$ is constant. The hardening rate is sensitive to temperature and plastic strain. There is a high degree of work hardening associated with the transformation from austenite to martensite.

Three characteristic regions, which define the hardening behavior of the austenitic stainless steel, are marked 1, 2 and 3 on the curve in Fig. 5. The first region between RT and 473 K is due to plentiful transformation of $\alpha'$ martensite. The second region is related to the hardening rate drops because $\gamma$ austenite to $\alpha'$ martensite transformation begins to slow down due to increase in deformation temperature. In third region drastic decrease in hardening rate is observed at temperatures above 623 K, because negligibly small amount of $\alpha'$ martensitic transformation occurred (as indicated by magnetic measurement), and the austenitic stainless steel may be considered as single $\gamma$ austenitic phase. By extrapolating the hardening rate from temperatures above 623 K, an approximate hardening rate of 0.475 can be obtained. This value is very close to the hardening rate of stainless steel (0.48) [27]. At temperatures above 623 K, the slope of the curve is almost zero, this means no work hardening effect at temperatures above

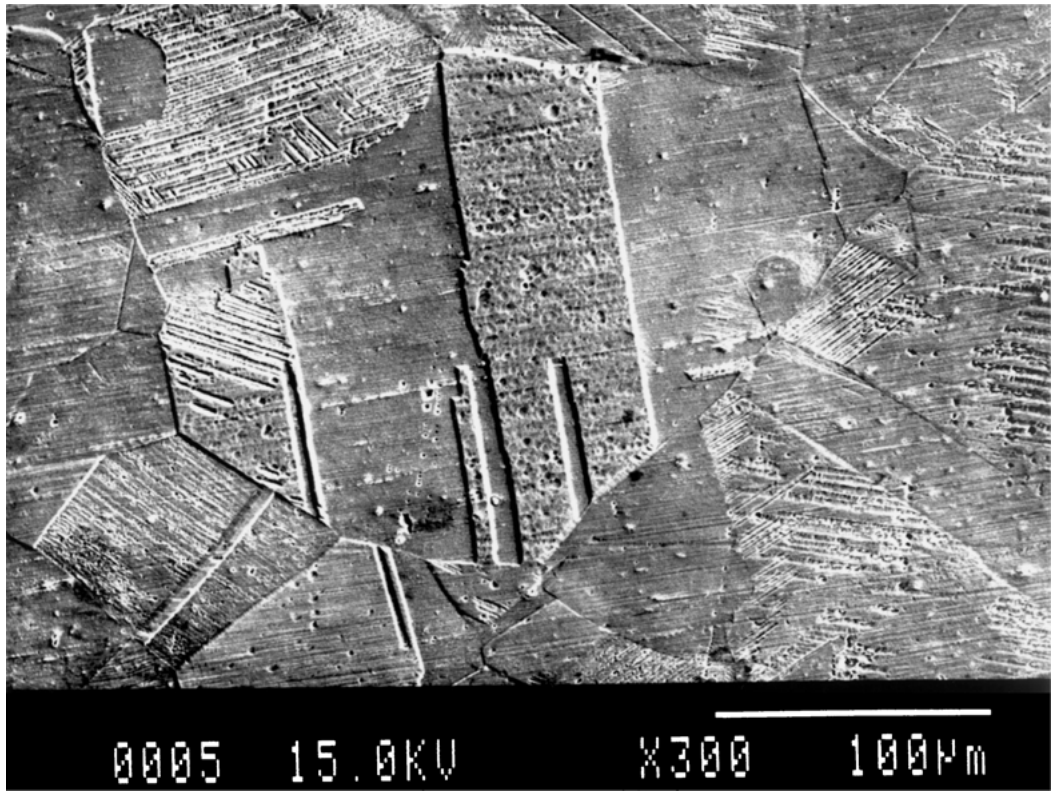


(a)

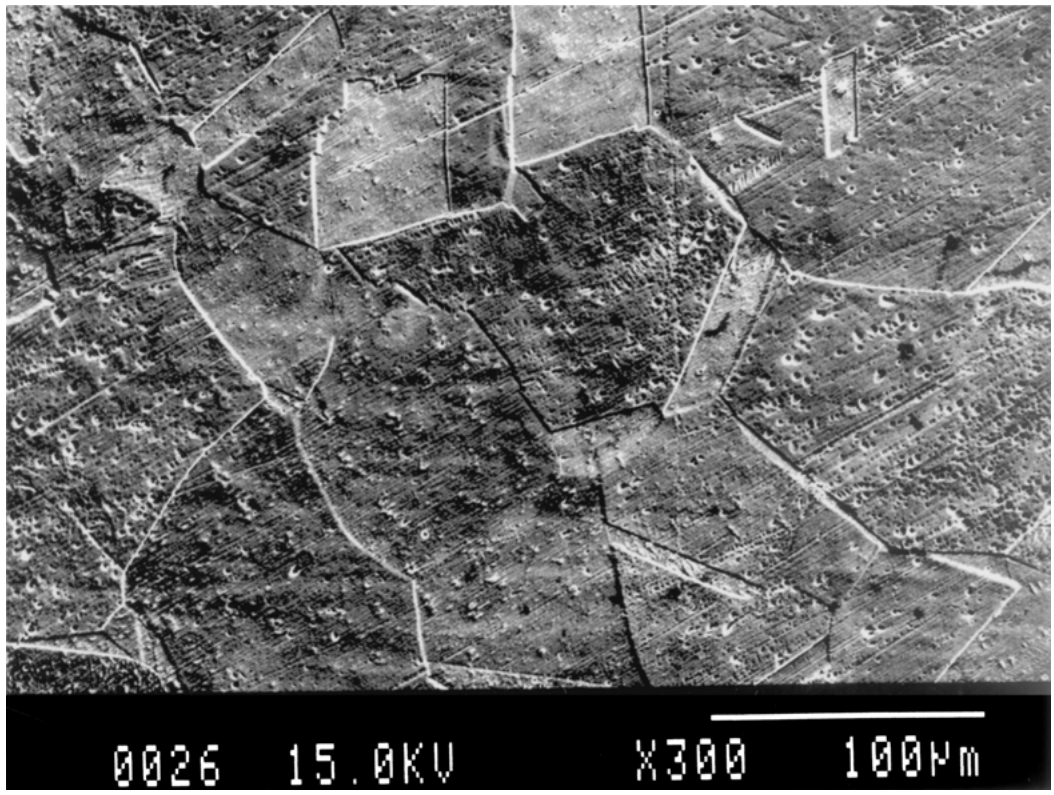


(b)

*Figure 6* SEM micrographs of specimens after compressive deformation to 40% plastic strain (a) at RT and (b) at 723 K.

623 K. At RT with larger plastic strains (above 40%) the transformation did not saturates (curve is not shown here) and the hardening rate still increased resulting in more transformation of $\alpha'$ martensite.

Fig. 6a and b show the scanning electron micrograph of specimens after compressively deformed to 40% plastic strain at RT and 723 K, respectively. Observations on a number of grains confirm that there are more streaks and bands at RT than at 723 K. The most conspicuous change is that no such streaks and bands are observed in the deformed specimens at temperatures above 623 K.

Because the experiments were conducted under compression, it was possible to study the austenite to

martensite transformation. The results from investigation lead to many important conclusions concerning the compressive deformation of austenitic stainless steel at various temperatures from 10 to 40% plastic strain.

The stress-strain slope depends on the slip, pile-ups of dislocations and volume percentage of $\alpha'$ martensitic transformation. At this point, it is interesting to revisit the stress-strain curves of Fig. 3. The stress-strain curves are similar, however, the slope of the curve after yield at RT deformation is steeper than that of the curve for specimens deformed at all of the temperatures. As shown in Fig. 3 the slope of the curves after yield at temperatures between 673 K and 723 K are almost constant. The presence of dislocation pile-ups has the role of increasing the slip resistance and hardening the matrix. Since this local pile-up of slips and bands are observed in SEM study of the specimen (Fig. 6a), it is believed to produce an ascending stress-strain curves rather than a linear line typically identified at deformation temperatures above 623 K.

## 3.2. Saturation magnetization and volume percentage of $\alpha'$ martensite

The magnetic property was obtained at RT in applied field of 0 to 30 kOe. The results of magnetization testing of specimens compressively deformed at various temperatures to 40% plastic strain are shown in Fig. 7a. Magnetization decreases with the increase of deformation temperatures from RT to 723 K. Fig. 7b shows the enlarge details of Fig. 7a at temperatures above 523 K. From Fig. 7b we can observe very low values of magnetization in the specimens before and after annealing without plastic deformation. Almost no effect of magnetic change is observed on specimens deformed at temperatures above 673 K, even after 40% plastic strain.

The saturation magnetization, which is proportional to the volume of ferromagnetic phase [15, 16] is obtained by extrapolating the linear part of magnetization curve back to zero applied magnetic field. In this system only $\alpha'$ martensite is ferromagnetic. A value of saturation magnetization of 154 emu/g corresponds to 100% $\alpha'$ martensite [28]. The volume percentage of $\alpha'$ martensite phase has been calculated from the saturation magnetization results. Fig. 8a and b (Fig. 8b is the enlargement showing details of Fig. 8a at temperatures above 523 K) show saturation magnetization and volume percentage of $\alpha'$ martensite as a function of temperature from 10 to 40% plastic strain condition. The values of saturation magnetization in the as-received and solution annealed specimens were 0.035 emu/g and 0.05 emu/g, respectively. Therefore, in the initial state there were already 0.02 and 0.03 volume percentage of $\alpha'$ martensite in the as-received and solution annealed specimens,

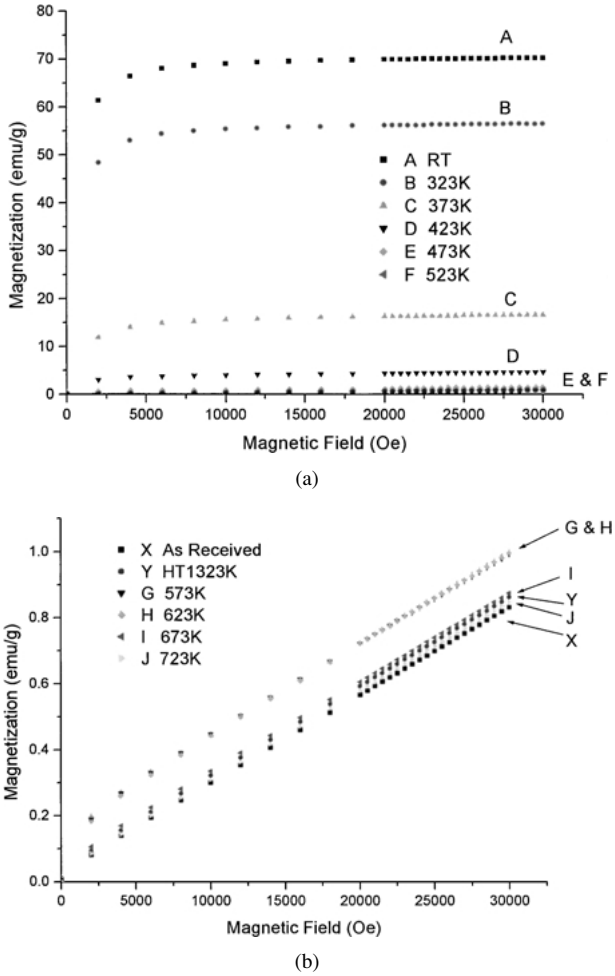


*Figure 7* (a) Magnetization as a function of magnetic field applied to specimens deformed at various temperatures to 40% plastic strain. (b) Enlargement showing details of (a) at temperatures above 523 K.

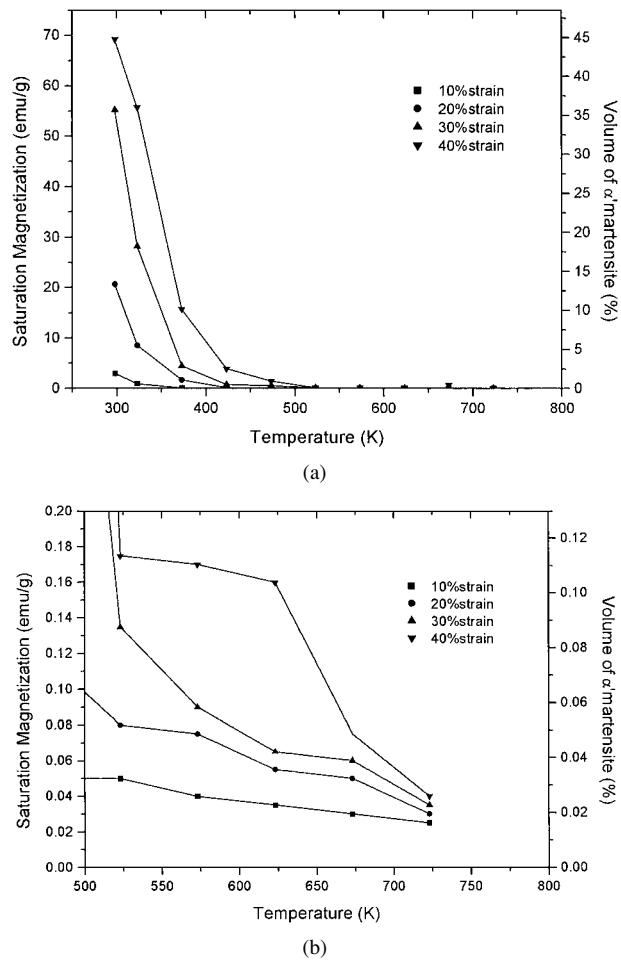


*Figure 8* (a) Saturation magnetization and volume percentage of $\alpha'$ martensite as a function of temperature. (b) Enlargement showing details of (a) at temperatures above 473 K.

TABLE III Magnetic properties and volume percentage of $\alpha'$ martensite in austenitic stainless steel after compressive deformation at various temperatures to 40% plastic strain

| Specimen no. | Deformation temp. (K) | Saturation magnetization (emu/g) | Volume % of $\alpha'$martensite | Coercive force (Oe) | | |
|---|---|---|---|---|---|---|
| | | | | X | Y | Z |
| SS-50 | As-received | 0.035 | 0.023 | | | |
| SS-51 | Sol. annealed | 0.050 | 0.033 | | | |
| SS-56 | RT | 69.00 | 44.81 | 42 | 40 | 78 |
| SS-60 | 323 | 55.50 | 36.04 | 50 | 49 | 96 |
| SS-64 | 373 | 15.70 | 10.20 | 77 | 74 | 128 |
| SS-68 | 423 | 3.900 | 2.533 | 95 | 95 | 145 |
| SS-72 | 473 | 1.425 | 0.925 | 115 | 117 | 181 |
| SS-76 | 523 | 0.175 | 0.114 | 190 | 200 | 220 |
| SS-80 | 573 | 0.170 | 0.111 | 108 | 96 | 80 |
| SS-84 | 623 | 0.160 | 0.104 | 60 | 60 | 50 |
| SS-88 | 673 | 0.075 | 0.049 | 40 | 48 | 48 |
| SS-92 | 723 | 0.040 | 0.026 | 42 | 40 | 38 |

respectively. Relevant data of magnetic properties and volume percentage of $\alpha'$ martensite are given in Table III.

In all the specimens after compressive deformation at temperatures below 673 K the coexistence of ferromagnetic and paramagnetic states are observed reasonably depending on the volume percentage of $\alpha'$ martensite phase. The value of saturation magnetization after compressive deformation to 40% plastic strain at RT is 69 emu/g, corresponding to 45 volume percentage of $\alpha'$ martensite. Below 623 K, $\alpha'$ martensite was detected after deformation to 10 to 40% plastic strain. The volume fraction of $\alpha'$ martensite depends on the temperature and level of plastic strain. From Fig. 8b, at 623 K with 40% plastic strain, the saturation magnetization is 0.16 emu/g, corresponding to 0.104 volume percentage of $\alpha'$ martensite phase. At temperatures above 623 K much less volume percentage of $\alpha'$ martensite was obtained. The specimens can be considered to be nearly completely paramagnetic at temperatures above 623 K; the values of saturation magnetization are comparable or lower than those of the as-received and solution annealed specimens. The same trend is also observed at different temperatures from 10% to 30% plastic strain. The saturation magnetization shows a remarkable decrease with increasing temperature.

The results of magnetic measurements suggest that martensitic transformation occurred at and below 623 K and the volume percentage of $\alpha'$ martensite depends on the plastic strain and deformation temperature.

Increasing the volume percentage of $\alpha'$ martensite in the specimens generally resulted in an increase in the stress, yield stress and hardening rate. It is believed that the increase is the result of microstructural features produced during compressive deformation. In Stage I (Fig. 3), hardening develops which indicates dislocation activity in the austenitic stainless steel. During Stage II the additional hardening is may be due to the increase of $\alpha'$ martensite volume fraction and blockage of further transformation by existing martensite boundaries. Specifically, the interaction of multiple slip systems and martensite laths leads to produce an ascending stress-strain curve rather than a linear line typically identified at deformation temperatures above 623 K. The $\alpha'$ martensite may be obtained in greater amount in the specimen compressively deformed at room temperature to 40% plastic strain.

The hardening of austenitic stainless steel is determined principally by the production, distribution and motion of dislocation and the amount of martensitic transformation. Generally the austenitic stainless steel is made harder by the presence of more dislocations and is made softer by fewer dislocations when there is only austenitic phase. The increased stress is caused by interaction of dislocations that reduces the mobility of the dislocations and consequently leads to hardening. There may be an additional strengthening effect due to the shear transformation from austenite to martensite. The hardening behavior also depends on the strength of obstacles developed due to the propagation of slip at the grain boundaries. This fact may result from differences in the amount of retained austenite and the differing conditions of martensitic transformation during deformation. The number of slip systems at deformation temperature 623 K to 40% plastic strain may produce little slip and hence low hardening in the specimen. At high temperatures above 623 K, there was no formation of $\alpha'$ martensite. Hardening of stainless steel may be explained as follows: In the elastic region, stress is accommodated by the increase or decrease in atomic spacing of the lattice. Potentially this spacing change always exists if the internal stress is not released, however at some critical stress value "slip systems" within the material are activated and the material begins plastic flow. As plastic deformation progresses, however, dislocation generation and interaction leads to work hardening. Since the generation of dislocations is closely related to the stacking fault energy, '$\gamma$', of austenite, it is clear that this parameter determines the rate of transformation during deformation.

Shramm and Reed [29] have established a relationship between stacking fault energy of the austenite and its chemical composition;

$$\gamma = -53 + 6.2 \text{ wt\% Ni} + 0.7 \text{ wt\% Cr} + 3.2 \text{ wt\% Mn} + 9.3 \text{ wt\% Mo mJ m}^{-2}$$

Nickel tend to raise the stacking fault energy thereby influencing dislocation cross slip while chromium,

manganese and silicon tend to decrease the stacking fault energy of the austenite. Accordingly, the value of stacking fault energy $\gamma$ for the stainless steel used in this work was about 15.27 mJ $m^{-2}$, which is very close to the value 18 mJ $m^{-2}$ obtained by Manganon and Thomas [19].

Because of the low stacking fault energy of the austenitic stainless steel, the formation of $\alpha'$ martensite may be facilitated by dislocations. Moreover, local stress concentrations are also believed to be the primary martensite nucleation sites. The difference of hardening rate obtained at low and high temperatures becomes significant due to substantial formation of $\alpha'$ martensite. The slips in the grain interior occur, whereas hardening rate rises due to increased poly slip activity in grains leads to pile up of dislocations near grain boundaries. Hardening rate lend further proof that the $\alpha'$ martensite volume fraction was increasing during the ascending portion of the stress-strain curve.

The stress decreases from 2023 MPa at RT to 953 MPa at 673 K when the plastic strain was 40%. The main reason for this difference is attributed to the fact that softening may occur at temperature 673 K and above even with 40% plastic strain, as no slips and other defects can be seen from Fig. 6b. The micro hardness (160 Hv) at 673 K was obtained which is nearly the same as micro hardness (150 Hv) of the as-received specimen. The micro hardness result also indicated the absence of $\alpha'$ martensite in the specimens at temperatures above 623 K. At high deformation temperature the dislocation can move over large distances, and depending on the type of dislocation, may mutually annihilate each other, climb or rearrange into more stable configurations [30]. In austenitic stainless steel, thermally activated dislocation relaxation process may occur at temperatures above 623 K. This relaxation process results in large decrease of dislocation density and decomposition of dislocation groups, and also the decrease of internal stresses [31]. The suppression of $\alpha'$ martensitic transformation is associated with increased mobility of extended dislocations at high temperature. Softening also may be due to the formation of sub-grains or re-crystallization of $\gamma$ austenitic phase. Furthermore, stacking fault energy increased with temperature and made $\alpha'$ martensite transformation difficult at temperatures above 623 K [32].

X-Ray diffraction was also used to determine the phases and contents in the specimens after compressive deformation. XRD patterns taken from the specimens deformed at different temperatures to 40% plastic strain are shown in Fig. 9, in comparison to the XRD pattern of as-received state. The volume percentage of $\alpha'$ martensite phase was calculated from the integrated intensity ratios of $\gamma$ and $\alpha'$ peaks. Table IV summaries all the phases detected and calculated volume percentage of $\alpha'$ martensite in as-received, solution annealed and the compressively deformed specimens at different temperatures.

It can be seen that the X-ray diffraction patterns for both as-received and compressively deformed specimens exhibits all $\gamma$ austenite peaks, but in case of compressively deformed specimens $\alpha'$ martensite peaks are also observed indicating that martensite phase generated in the specimens in the process of deformation at different temperatures. The X-ray diffraction pattern of solution-annealed specimen (not shown here) is exactly like as-received specimen. For specimens deformed at different temperatures a high intensity of $\gamma$ austenite peak is observed in the (111) plane. It is also observed that with the increase in deformation temperature there is decrease in intensity and broadening of $\gamma$ austenite peaks in the (200), (220) and (311) planes.

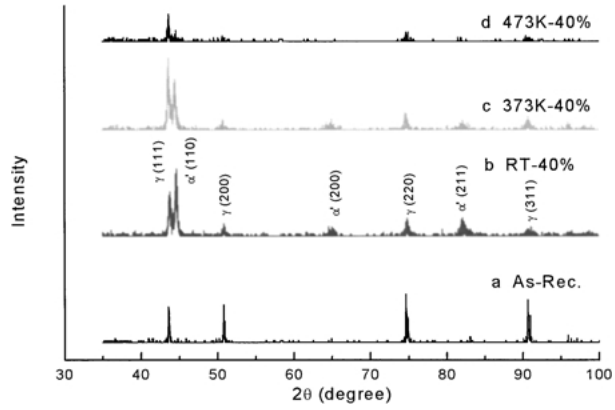


*Figure 9* X-ray diffraction patterns of austenitic stainless steel specimens after compressive deformation to 40% plastic strain. (a) as-received, (b) at RT, (c) at 373 K and (d) at 473 K.

The deformation at RT causes a prominent increase in peak intensity of $\alpha'$ martensite at diffraction angle of $2\theta = 44.32$ or (110) plane. The deformation at RT also causes an increase in the intensity of $\alpha'$ martensite peak in (200) and (211) planes. The intensity of $\alpha'$ martensite peak decreases with the increase of deformation temperature. In the X-ray diffraction patterns $\alpha'$ martensite phase is seen to be present in traces and are hardly discernable after deformation at temperature above 473 K. Generally, the quantification by X-ray diffraction in the specimen with lower than 2 volume percentage of $\alpha'$ martensite is not possible. The X-ray diffraction patterns show that there exists no other phases.

The magnetic measurement results show that $M_d$ (the temperature above which stresses cannot initiate transformation) is a strong function of deformation temperature. In this work, the formation of $\alpha'$ martensite in austenitic stainless steel was observed by compressive deformation below 673 K or by magnetic measurements the absence of $\alpha'$ martensitic phase was observed at temperatures above 623 K. Thus the $M_d$ temperature of austenitic stainless steel used in this work is estimated to be below 673 K.

### 3.3. Coercive force and $\alpha'$ martensite

Magnetic properties are not only depend on the volume percentage of $\alpha'$ martensitic phase, but also on numerous other parameters which determine the form of martensite on micro-scale, such as size, shape, distribution, degree of randomness and coherency in the austenitic matrix. Although the austenitic stainless steel is essentially isotropic, anisotropy does arise due to deformation and martensitic transformation. The coercive

TABLE IV Phase detection and volume percentage of $\alpha'$ martensite by XRD in austenitic stainless steel after compressive deformation at different temperatures to 40% plastic strain

| Specimen no. | Deformation temp. (K) | Volume % of $\alpha'$ martensite | Phases |
|---|---|---|---|
| SS-50 | As-received | – | $\gamma$ (111), $\gamma$ (200), $\gamma$ (220), $\gamma$ (311), |
| SS-51 | Sol. annealed | – | |
| SS-56 | RT | 51.62 | $\gamma$ (111), $\gamma$ (200), $\gamma$ (220), $\gamma$ (311), $\alpha'$ (110), $\alpha'$ (200), $\alpha'$ (211), |
| SS-64 | 373 | 37.46 | $\gamma$ (111), $\gamma$ (200), $\gamma$ (220), $\gamma$ (311), $\alpha'$ (110), $\alpha'$ (200), $\alpha'$ (211), |
| SS-72 | 473 | 4.167 | $\gamma$ (111), $\gamma$ (200), $\gamma$ (220), $\gamma$ (311), $\alpha'$ (110), $\alpha'$ (211)*, |

*Note*: *denotes traces.

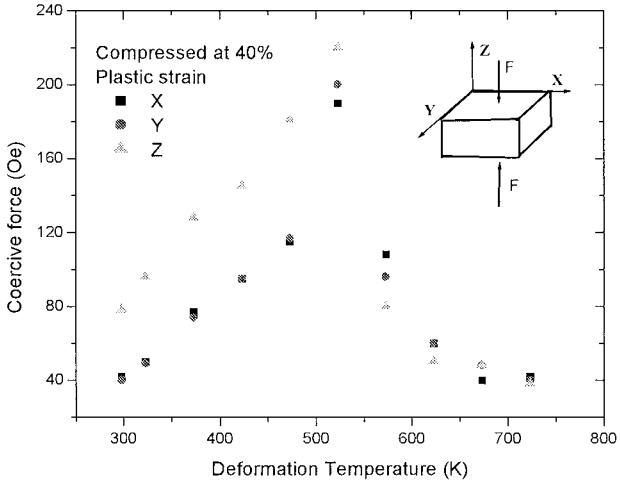


*Figure 10* Coercive force as a function of temperature after compressive deformation to 40% plastic strain.

force is derived from magnetic hysteresis loop measurements performed using a VSM magnetometer. Fig. 10 shows the coercive force measurement result in the specimens after compressive deformation to 40% plastic strain at various temperatures. From the Fig. 10, we can see that the coercive force is exclusively connected with the size, shape and spatial distribution of martensite.

The measurements were performed in three directions for each specimen, parallel to compressive direction (Z), perpendicular to the surface of the specimen (Y), and perpendicular to Y and Z (X) as shown in Fig. 10. The coercive force depends on the magnetization direction and the results are shown in Table III. The coercive force for Z direction ranges from 38 to 220 Oe, and the values are much higher as compared with the values in X and Y directions at temperatures below 523 K. What attracts our attention is that coercive force increases with the increase of deformation temperature, after reaching a maximum value of 220 Oe at temperature of 523 K, then it rapidly decreases to a very small value, which is nearly the same as in X and Y directions. But at temperatures above 523 K the value of coercive force in Z direction are lower than or comparable in X and Y directions.

Deformation at various temperatures and plastic strain level can lead to a number of changes that may alter magnetic behavior: (i) size, shape and distribution of transformed $\alpha'$ martensite phase (ii) an increase in the number of microscopic pinning sites in the form of dislocation tangles, may act as an obstacles to domain wall movement, (iii) development of a crystallographic texture, which may alter the magnetic easy axis, direction and (iv) additional, local internal stress increases in plastic region associated with the work hardening processes of the specimens.

For ferromagnetic materials, the coercive force $H_c$ is the maximum resistance force against domain wall movement. The coercive force is given by

$$H_c = \frac{1}{2M_s F \cos\phi}\left(\frac{\partial E_\omega}{\partial x}\right)_{\max} \quad (2)$$

where $M_s$ is the saturation magnetization. $F$ is the total area of the domain wall in the unit volume. $\phi$ is the angle between the normal of the domain wall and the external magnetic field $H$. $E_\omega$ is the domain wall energy depending on the position and results from the strain field of lattice defects. It has been found that in low carbon steels, $(\partial E_\omega/\partial x)_{\max}$ is in proportion to dislocation density $\rho^{1/2}$ [15, 33].

An unmagnetized martensitic phase transformed specimens may contain randomly arranged magnetic domain. As specimen gets magnetized by an applied field, the domains tend to align with the field. Coercive force was both due to the interaction between domains, which tends to align the domains in the magnetized direction, and to impediments to the domain rearrangement caused by structural irregularities or pinning sites.

The effect of grain boundaries on magnetic properties have been studied by many scientists [33, 34]. Their results may cast light on the non-destructive evaluation of austenitic stainless steel. The grain boundary acts as an obstacle to the movement of domain wall. Domain wall energy $E_\omega$ is influenced by the different atomic structure of the grain boundary. Coercive force and the initial susceptibility depend on the grain size. The effect of grain boundary on magnetic properties can be separated into three cases [34]:

(i) the grain size is sufficiently large enough ($>0.1$ $\mu$m) for the domain wall to move in the grain.
(ii) the grain size is equivalent to the thickness of the domain wall and,
(iii) the grain size is much smaller than the thickness of the domain wall ($<0.1$ $\mu$m).

Therefore, in the case (i) where the grain size is large have less grain boundary area and in the case (iii) where grain size is small have large grain boundary area and less energy. In both cases of (i) and (iii) the grain boundary may not form hard obstacle for the movement of domain wall, therefore the coercive force may not show

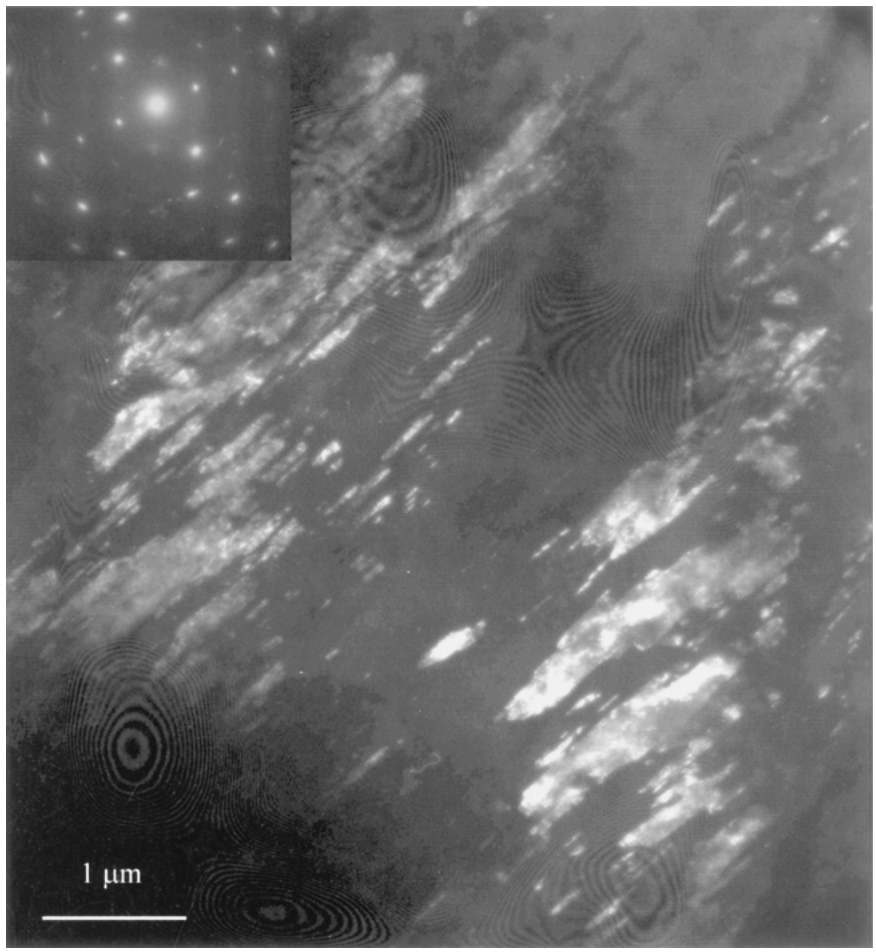


(a)

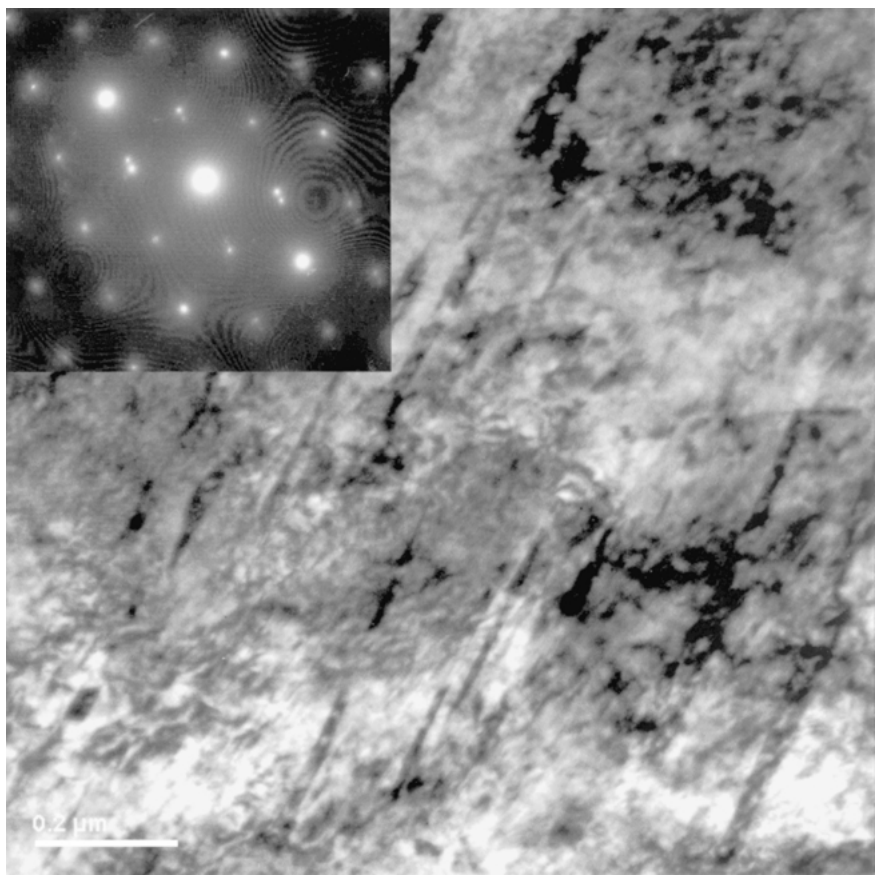


(b)

*Figure 11* TEM dark-field micrographs and selected-area diffraction patterns of austenitic stainless steel specimens after compressive deformation to 40% plastic strain. (a) at RT, (b) at 373 K, (c) at 473 K, (d) at 573 K and (e) at 673 K. (*Continued*)

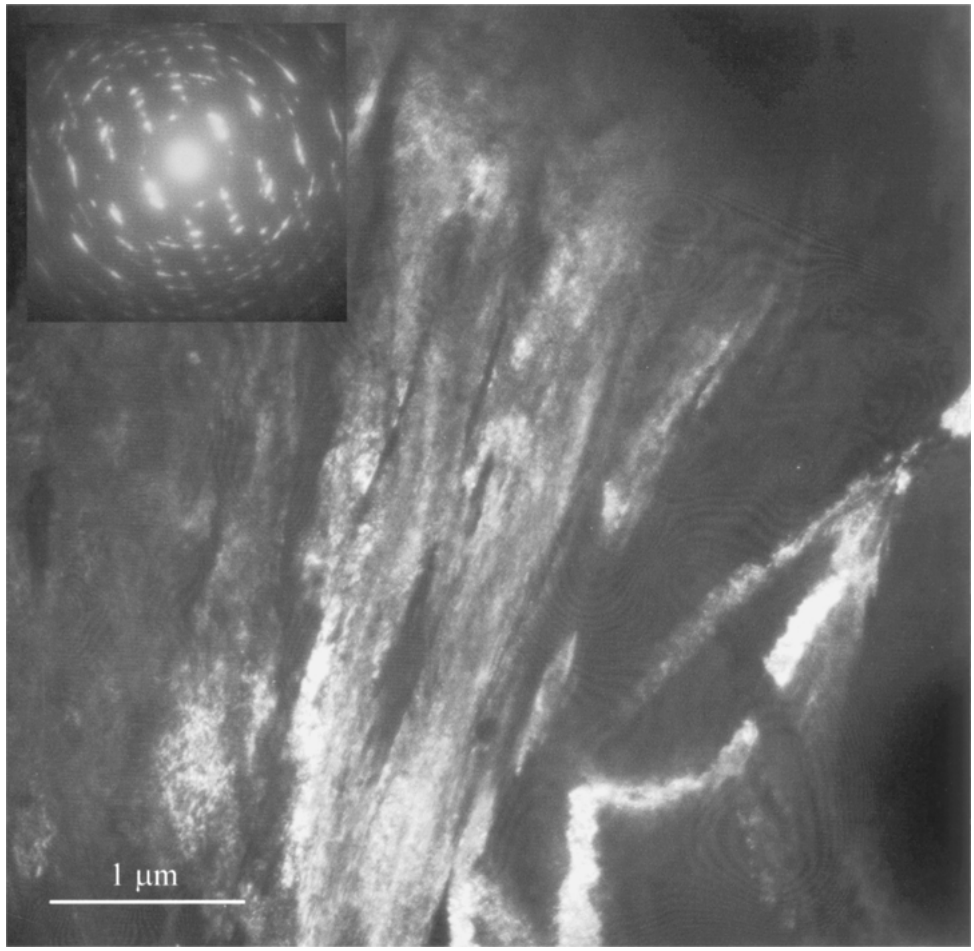


(c)

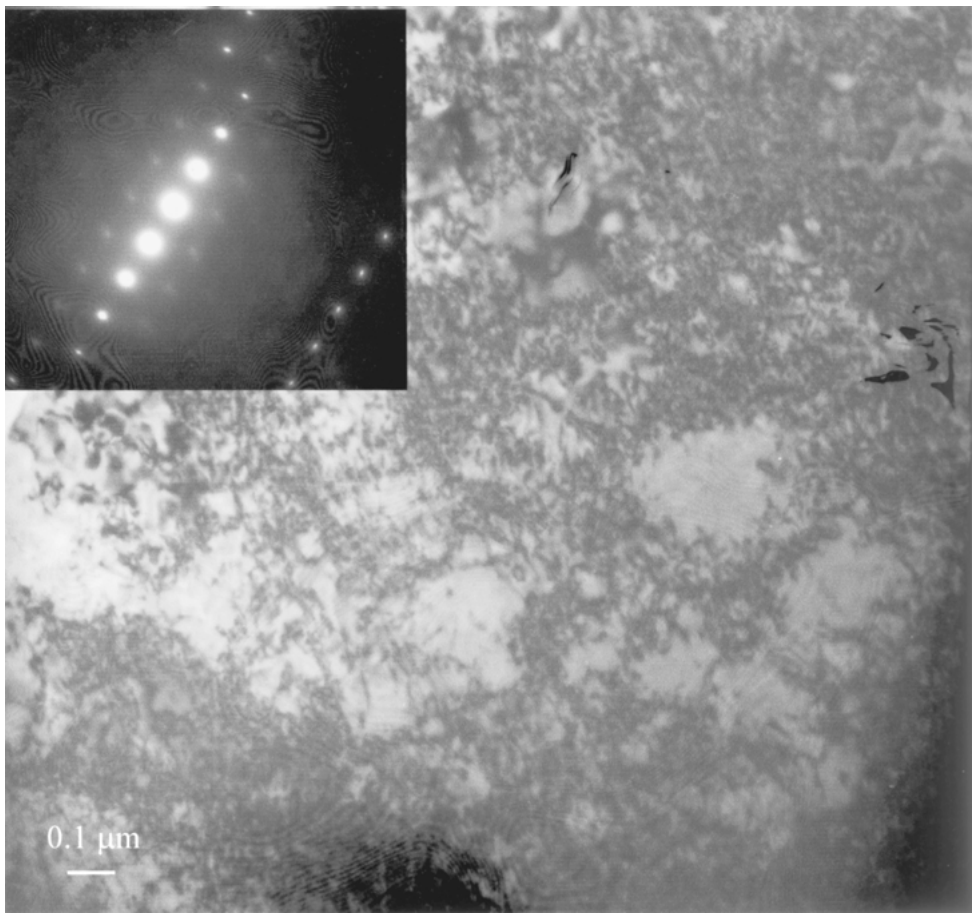


(d)

*Figure 11* (*Continued*).

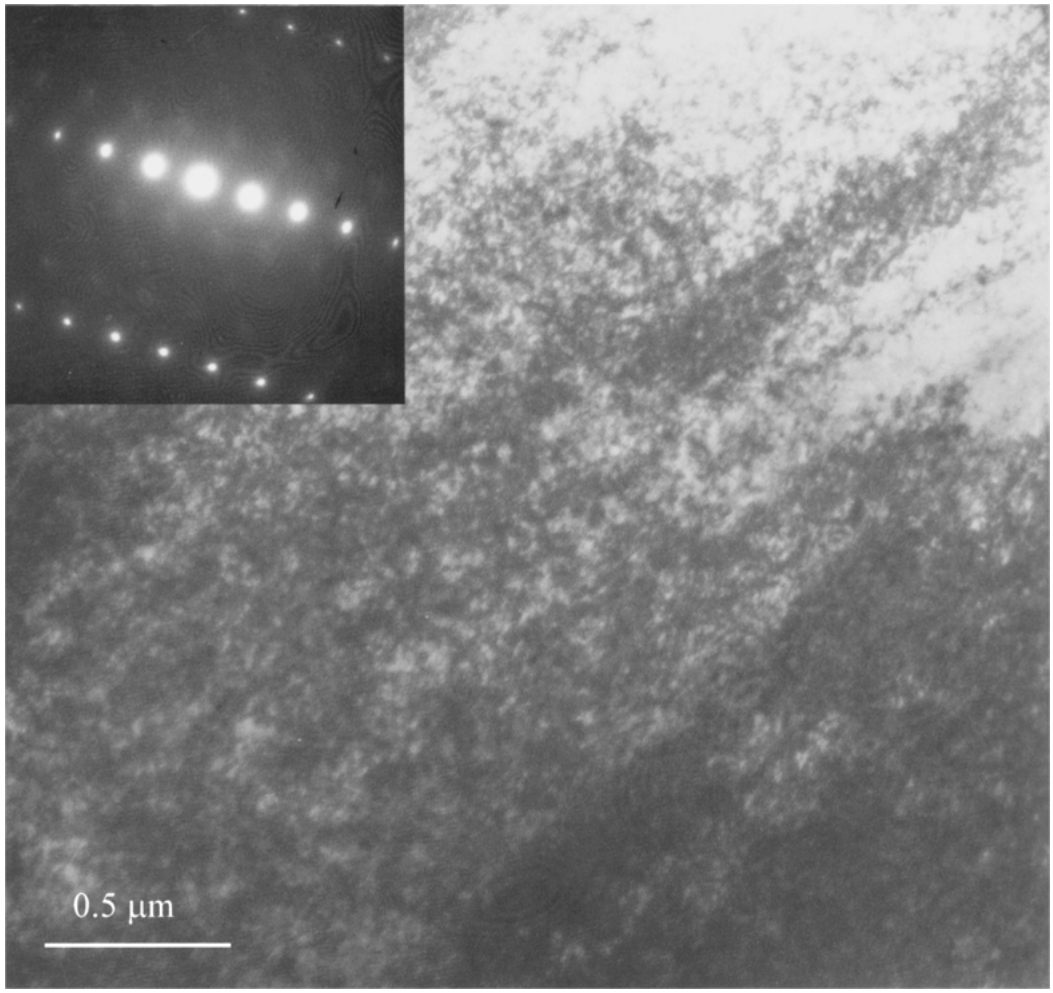


(e)

*Figure 11* (*Continued*).

high value. However, for case (ii), the domain wall may be pinned by grain boundary and may exhibit high value of coercive force.

Now let us discuss about the effect of grain boundary on coercive force in ferromagnetic materials. The deflection of moments exists along the grain boundary at the triple point where three grains contact and at the other multiple point where more than four grains contact each other. The domain wall will receive the forces of $f_a$, $f_t$ and $f_m$ in the grain boundary, the triple point, and the multiple point, respectively. The forces depend on the relative crystal orientation of the grains. The maximum force of the domain wall by the grain boundaries is given by

$$\left(\frac{\partial E_\omega}{\partial x}\right)_{\max} = \frac{k_1\langle f_a\rangle}{a^2 d} + \frac{k_2\langle f_t\rangle}{a d^2} + \frac{k_3\langle f_m\rangle}{d^3} \quad (3)$$

where $d$ is the mean diameter of the grain, $k_1, k_2$ and $k_3$ are constants depending on the shape of the grain boundary, and a is the lattice constant. The second and third term are negligible compared with the first one and the coercive force is given by substituting Equation 3 into 2, we get

$$H_c = \frac{k_1\langle f_a\rangle}{2M_s a^2 F\cos\phi} \cdot \frac{1}{d}. \quad (4)$$

$H_c$ is inversely proportional to the grain size $d$. This relation coincides with the experimental results of $\alpha$-Fe metal [15].

If we suppose that each $\alpha'$ martensitic lath is a grain. We can get the size of $\alpha'$ martensite from TEM micrographs. Figs 11a–e show the micrographs of specimens deformed to 40% plastic strain at RT, 373 K, 473 K, 573 K and 673 K, respectively. From the micrographs the size of $\alpha'$ martensite transformed at different temperatures are: (a) at RT, about 0.8–1.0 $\mu$m in length and 0.1–0.3 $\mu$m in width, (b) at 373 K, about 0.2–0.5 $\mu$m in length and 0.01–0.04 $\mu$m in width, (c) at 473 K, the size becomes difficult to be measured, we can guess from the diffraction pattern, that the size may be around 0.05–0.1 $\mu$m, (d) at 573 K the martensite size becomes too small, falls into nanometer scale (<100 nm), magnetic measurement shows the volume percentage of $\alpha'$ martensite is low (0.12%) however, diffraction pattern can not reveal their existence and (e) the micrograph clearly indicate the presence of well developed cell structure in the austenitic phase. The only presence of austenite is indicated by diffraction pattern and by magnetic measurements. The microstructure of $\alpha'$ martensite was changes from lath to fine needle and finally cell structure of austenite [Fig. 11a–e]. The morphology of which was dependent on the deformation temperature and level of plastic strain.

The result about the size of $\alpha'$ martensite lath obtained from TEM reveals that, in austenitic steel, the coercive force also follows the relationship similar to that of for ferromagnetic materials such as $\alpha$-Fe metal. And it has good coincidence with the results obtained in magnetic films.

Anisotropy in coercive force of the austenitic stainless steel specimens shown in Fig. 10 is due to the shape and size of $\alpha'$ martensite. When compressive deformation takes place, the induced martensite phase forms on $\{111\}_{fcc}$ habit slip planes at 45° to the compression direction. As the deformation continues further, the previous habit planes become hard due to the pile up of dislocations, and may rotate to another position that is preferred to the direction perpendicular to the compression. Meantime the martensite laths may also rotate with the rotation of slip planes. Then new slip planes start at 45° to the compressive direction. If the compressive stress is high enough, secondary slip planes cut the long $\alpha'$ martensite laths formed on the previous habit planes to short. Therefore, shape of $\alpha'$ martensite lath is long in the direction perpendicular to compression and short along compression, as shown in TEM micrographs.

The temperature dependence of coercive force is due to the easiness of activation of slip systems and movement of dislocations. At low temperature, it requires larger external energy than at higher temperature to active the habit slip planes and therefore less slip systems are activated. Activation of less slip systems and higher plastic strain produced lath martensite at low temperature. While at higher temperatures, activation of more slip systems cut the martensitic phase to thin needles.

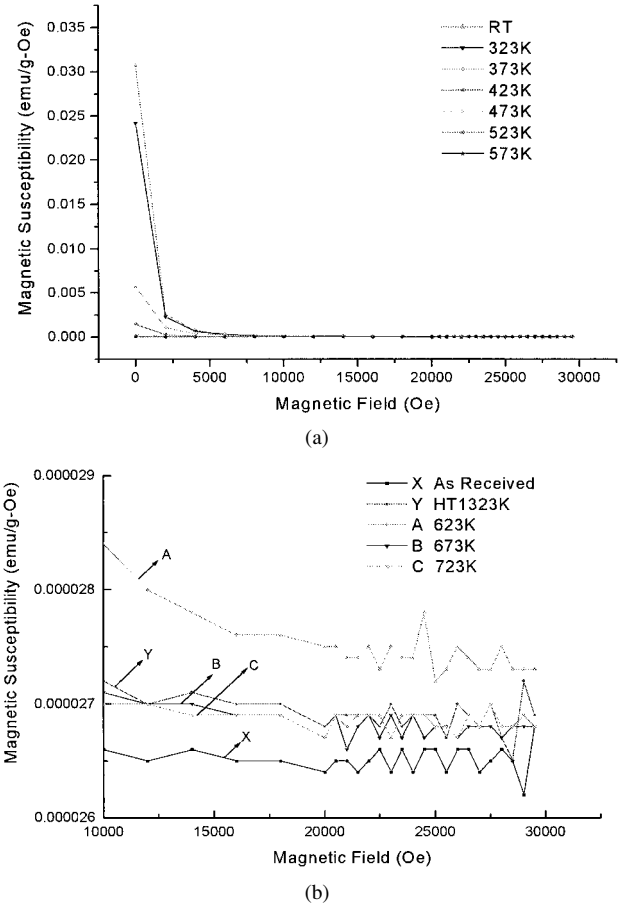


*Figure 12* (a) Magnetic susceptibility as a function of magnetic field for the specimens compressively deformed at various temperatures to 40% plastic strain. (b) Enlargement showing details of (a) at temperatures above 573 K.

## 3.4. Magnetic susceptibility

The magnetic susceptibility is highly structure sensitive [15], so that it may be used to investigate the ferromagnetic phase changes occurring due to compressive deformation at various temperatures. In case of ferromagnetic phase the value of magnetic susceptibility is strongly dependent on magnetic field strength. The magnetic susceptibility is defined as the ratio of magnetization to magnetic field strength.

Fig. 12 shows measurement results of the magnetic susceptibility as a function of magnetic field for the austenitic stainless steel specimens after compressive deformation at various temperatures to 40% plastic strain. Austenitic stainless steel exhibited an appreciable change in the magnetic susceptibility when they were subjected to compressive deformation at various temperatures. As understood from the Fig. 12, magnetic susceptibility is decreases with increasing temperature. The specimen deformed at RT to 40% plastic strain has a large value of magnetic susceptibility (Fig. 12a). While that of specimen deformed at 623 K to 40% plastic strain the value of magnetic susceptibility is about $2.75 \times 10^{-5}$ emu/g-Oe as shown in Fig. 12b (enlarge scale of Fig. 12a). The magnetic susceptibility increases with plastic strain at constant temperature. As can be seen, a plastic strain of 40% up to 623 K, show magnetic susceptibility and ferromagnetism are observed in the magnetization curves due to $\alpha'$ martensitic transformation. Moreover, it is known from Fig. 12b that the magnetic susceptibility at temperatures above 673 K to 40% plastic strain is lower than those of solution annealed specimen which shows no magnetic transition and hence no $\alpha'$ martensitic transformation.

The factors that contributes to hardening of the specimens and hence to increase yield strength, are also the factors that affect the motion of magnetic domain walls. Therefore, correlation may be observed between some of the structure sensitive magnetic properties and the dislocations. Magnetic measurements revealed the presence of very low volume percentage of $\alpha'$ martensite at 623 K. The volume percentage of $\alpha'$ martensitic transformation which is calculated from the value of saturation magnetization primarily depends on the level of plastic strain and temperature. In weakly magnetic materials such as paramagnets or diamagnets the value of magnetic susceptibility $\alpha'$ is approximately zero. It seems that low magnetic susceptibility at temperatures above 623 K are due to the disappearance of martensitic phase.

## 4. Conclusions

1. The slope of stress-strain curve after yield for RT deformation is steeper than that of the curves for specimens deformed at all of the temperatures. The slope of

the curves at temperatures between 673 K and 723 K after yield are almost constant. The yield stress decreased with the increase of deformation temperature. Compared to the RT deformation, for the deformation at temperatures above 623 K, yield stress decreased drastically. Hardening rate also decreases with the increase of deformation temperature.

2. Magnetization decreases with the increase of deformation temperatures between RT and 723 K. Almost no effect of magnetic change is observed on specimens deformed at temperatures above 673 K, even after 40% plastic strain. The magnetic measurements show that martensitic transformation occurs at and below 623 K and the percentage of martensite depends on percentage of plastic strain and deformation temperature.

3. The coercive force was exclusively connected with size, shape and spatial distribution of martensite. High percentage of plastic strain produced lath like martensite at low temperature. While at higher temperatures thin needles were formed. The coercive force also depends on the magnetization direction and much higher value of coercive force is obtained in the direction parallel to compressive direction.

4. The specimen deformed at RT to 40% plastic strain has a large value of magnetic susceptibility. Magnetic susceptibility was decreased with increasing temperature.

## References


1. W. WEBER, K. L. FEISTE, W. REIMCHE and D. STEGEMANN, Characterization of Material Degradation and Detection of Imperfections inside of Thick Walled Austenitic Components with Electromagnetic Testing, The 10th International Symposium on Applied Electromagnetics and Mechanics, May 13–16, 2001, Tokyo, Japan.
2. K. HIDE, T. ONCHI, M. MAYUZUMI, K. DOHI and Y. FUTAMURA, *Corrosion* **51**(10) (1995) 757.
3. S. R. CHEN, H. A. DAVIES and W. M. RAINFORTH, *Acta Mater.* **47**(18) (1999) 4555.
4. A. KOHYAMA, M. L. GROSSBECK and G. PIATTI, *J. Nuc. Mater.* **191–194** (1992) 37.
5. F. A. GARNER, F. ABE and T. NODA, *ibid.* **155–157** (1992) 870.
6. N. HASHIMOTO, S. J. ZINKLE, A. F. ROWCLIFF, J. P. ROBERTSON and S. JITSUKAWA, *ibid.* **283–287** (2000) 528.
7. P. BALLO and V. SLUGER, Modelling of Irradiation Embrittlement in Pressure Vessels Steels, Proceedings of The 4th Japan-Central Europe Joint Workshop on Energy and Information in Non-Linear Systems, November 10–12, 2000, Brno, Czech Republic.
8. J. M. MCCARTHY and F. A. GARNER, *J. Nuc. Mater.* **155–157** (1988) 877.
9. E. L. HALL and C. L. BRAINT, *Metallurgical Transactions A* **15A** (1984) 793.
10. P. KAUPPINEN and J. SILLAMPAA, *The International Journal of Pressure Vessels and Piping* **54** (1993) 523.
11. P. KAUPPINEN and P. SARKINIEMI, *ibid.* **55** (1993) 141.
12. J. R. BOWLER, Recent Advances and Challenges in Eddy Current Non Destructive Evaluation Techniques, The 10th International Symposium on Applied Electromagnetics and Mechanics, May 13–16, 2001, Tokyo, Japan.
13. T. TANIGUCHI, K. NAKAMURA, D. KACPRZAK, S. YAMADA and M. IWAHARA, Eddy-Current Testing Image Processing for Extraction of Orientation of Defects The 10th International Symposium on Applied Electromagnetics and Mechanics, May 13–16, 2001, Tokyo, Japan.
14. S. TAKAHASHI, T. UEDA, J. ECHIGOYA and K. MUMTAZ, NDE by Magnetic Methods in SUS 304 Stainless Steel, Proceedings of The 4th Japan-Central Europe Joint Workshop on Energy and Information in Non-Linear Systems, November 10–12, 2000, Brno, Czech Republic.
15. S. TAKAHASHI, J. ECHIGOYA and Z. MOTOKI, *J. Appl. Phys.* **87**(2) (2000) 805.
16. S. TAKAHASHI, J. ECHIGOYA, T. UEDA, X. LI and H. HATAFUKU, *J. Mater. Processing Technol.* **108** (2001) 213.
17. S. S. HECKER, M. G. STOUT, K. P. STAUDHAMMER and J. L. SMITH, *Metall. Trans. A* **3A** (1982) 619.
18. C. J. GUNTER and R. P. REED, *Transactions of The ASM* **55** (1962) 399.
19. P. L. MANGONON JR. and G. THOMAS, *Metall. Trans.* **1** (1970) 1577.
20. J. W. BROOKS, M. H. LORETTO and R. E. SMALLMAN, *Acta Metall.* **271** (1979) 829.
21. T. MAKI and C. M. WAYMAN, *ibid.* **25** (1977) 681.
22. H. WARLIMONT, *Metall. Trans.* **2** (1971) 1847.
23. P. M. KELLY and J. NUTTING, *J. Iron Steel Inst.* **184** (1961) 199.
24. R. LANGEBORG, *Acta Metall.* **12** (1964) 823.
25. T. SUZUKI, H. KOJIMA, K. SUZUKI, T. HASHIMOTO and M. ICHIHARA, *ibid.* **25** (1977) 1151.
26. H. SEHITOGLU, I. KARAMAN, R. ANDERSON, X. ZHAG, K. GALL, H. J. MAIER and Y. CHUMLYAKOU, *Acta. Mater.* **48** (2000) 3311.
27. H. SUNADA, "Ensyu/Zairyo Shiken Nyumon, (Practice/Introduction of Materials)" (Taiga Syuppan, Tokyo, 1st Published on March 25, 1987, Republished on Sept. 1, 1991).
28. M. B. STEARNS, *Physical Rev.* **13** (1976) 1183.
29. R. E. SHRAMM and R. P. REED, *Met. Trans.* **6A** (1975) 1345.
30. D. DULL, "Introduction to Dislocations" (Pergamon Press, London, 1968) p. 245.
31. A. E. BERKOWITZ and E. KNELLER, "Magnetism and Metallurgy" (Academic Press, New York, 1969) p. 695.
32. F. ABRASSART, *Met Trans.* **4** (1973) 2205.
33. G. HERZER, *Physica Scripta* **T49** (1993) 307.
34. M. E. MCHENERY and D. E. LAUGHLIN, *Acta Mater.* **48** (2000) 223.



*Received 13 November 2002*
*and accepted 5 May 2003*